Interactions of Amino Acids and Polypeptides with Metal Oxide Nanoparticles Probed by Fluorescent Indicator Adsorption and Displacement

Sweccha Joshi,[†] Indrajit Ghosh,[†] Suman Pokhrel,[‡] Lutz Mädler,[‡,*] and Werner M. Nau[†,*]

[†]School of Engineering and Science, Jacobs University Bremen, Campus Ring 1, D-28759 Bremen, Germany, and [‡]Foundation Institute of Materials Science, Division of Process & Chemical Engineering, Department of Production Engineering, University of Bremen, Badgasteiner Str. 3, D-28359 Bremen, Germany
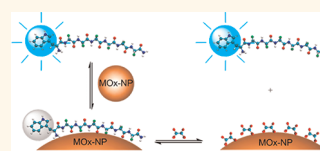
The size of nanoparticles (1−100 nm) is commensurate to those of important biological components, and consequently, there is a high probability that these nanoparticles interact with biomolecules (*e.g.*, DNA, proteins, cell membranes, *etc.*) and interfere with cellular processes.[1−4] In particular, metal oxide nanoparticles (MOx-NPs) have come into the focus of biological studies[5−8] because they are already being used for numerous commercial applications,[9−14] owing to their extremely high surface areas and various morphologies possessing numerous reactive surface sites.

Upon contact with biological matrices, most nanoparticles are coated by proteins.[15] A better understanding of such interactions at the "nano-bio" interface requires knowledge of absolute and relative adsorption propensities of amino acids, peptides, and proteins with MOx-NPs. Not surprisingly, several approaches have been undertaken, both experimentally and theoretically, to investigate adsorption of molecules on the surface of metal oxides[16−26] as well as to understand the effect of metal oxides on the fluorescence of proteins.[27−29] The complex structure and multiple binding motifs of proteins and the influence of the physical and chemical properties of the nanoparticles, including size, shape, surface charge (zeta-potential), solubility, and reactive surface groups, can lead to large variations in interactions in different environments (terrestrial, aquatic, *etc.*).[30,31] Methods that allow a rapid and convenient testing of such interactions remain therefore in high demand.

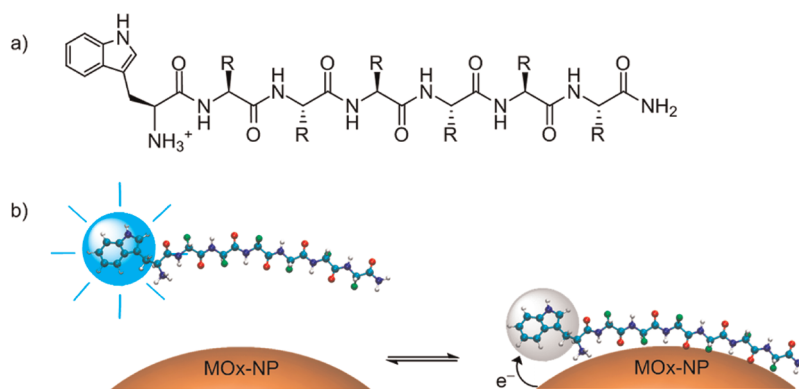In this study, we used optical spectroscopy to monitor the interactions of short polypeptides with MOx-NPs (Scheme 1). The method employs fluorescence quenching of tryptophan (Trp) and its derivatives[32] to monitor adsorption as well as desorption of Trp-labeled peptides to and from MOx-NPs. For this purpose, we have transferred the conveniently accessible indicator displacement method,[33−35] which is popular in biological and supramolecular chemistry,

ABSTRACT The adsorption of polypeptides containing an N-terminal tryptophan (Trp) residue attached to a hexa-backbone of alanine, serine, lysine, histidine, and aspartate was investigated by monitoring the fluorescence response of the Trp chromophore upon titration with metal oxide nanoparticles (MOx-NPs: CuO, Co_3O_4, TiO_2, MgO, and CeO_2). After correction for light-scattering effects, a strong static fluorescence quenching was observed upon addition of CuO and Co_3O_4 to the peptides. The interaction of MOx-NPs with the peptides was assigned to an adsorption of the peptide backbone on the nanoparticle surface. The method was refined using a derivatized amino acid, 5-fluoro-Trp (5F-Trp), which resulted in a stronger fluorescence response. The use of the fluorescent amino acid labels allowed the direct assessment of the adsorption propensities of Trp-containing peptides in dependence on the backbone, which was verified by zeta-potential measurements. Moreover, upon addition of different analytes to nanoparticles with preadsorbed Trp-containing polypeptides, adsorption propensities of the analytes were assessed by an indicator displacement strategy; that is, addition of increasing amounts of analyte resulted in a continuous fluorescence enhancement/recovery. This method afforded adsorption propensities for several analytes. The relative binding constants for the MOx-NPs, obtained from the competitive titrations, varied by more than 6 orders of magnitude for CuO (5F-TrpHis$_6$-NH$_2$ > TrpAsp$_6$-NH$_2$, TrpSer$_6$-NH$_2$ > TrpLys$_6$-NH$_2$, Trp, 5F-Trp > TrpAla$_6$-NH$_2$) but only 4 for Co_3O_4 (TrpHis$_6$-NH$_2$, TrpAsp$_6$-NH$_2$ ≫ TrpLys$_6$-NH$_2$, TrpAla$_6$-NH$_2$, TrpSer$_6$-NH$_2$, Trp, 5F-Trp). The study reveals that MOx-NPs adsorb biomolecular analytes with high selectivity, which has immediate implications for their applications in protein purification, drug delivery, and, potentially, for the assessment of their toxicology.

KEYWORDS: metal oxide nanoparticles · peptides · indicator displacement · adsorption · fluorescence · catalysis

Scheme 1. (a) General chemical structure of the model polypeptide with N-terminal Trp and amidated C-terminus. The residues R represent the amino acid side chains (for chemical structures, see Table 2). (b) Fluorescence response of Trp-containing polypeptides upon adsorption to metal oxide nanoparticles, with electron transfer being the proposed quenching mechanism.
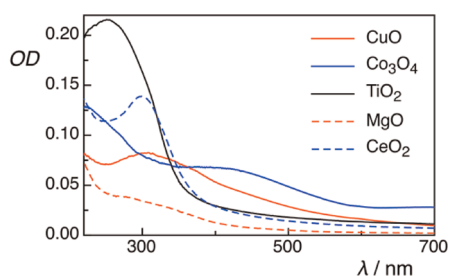

Figure 1. UV−vis spectra of selected metal oxide nanoparticles (0.01 mg mL^{-1}), in water at pH 7.

TABLE 1. Specific Surface Areas, Average Particle Sizes (Dry and in Solution), and Zeta-Potential Values of the Nanoparticles

MOx-NPs	SSA (m^2 g^{-1})^a	d_{BET} (nm)^b	d_h (nm)^{c,d}	ζ_{obs} (mV)^{d,e}
CuO	87	11	820	22
Co$_3$O$_4$	132	8	670	10
TiO$_2$	123	10	550	-17 ± 5
MgO	122	13	530 ± 310	14
CeO$_2$	164	5	280	-27

^{a} Specific surface area (surface area/mass) of MOx-NPs prepared using flame spray pyrolysis (FSP). ^{b} Average diameter of spherical particles calculated using the equation $d_{BET} = 6/(\rho \times SSA)$ (ρ, theoretical density). ^{c} Average particle diameter, calculated using the Stokes−Einstein equation, $D = k_b T/(3\pi\eta d_h)$ (D, diffusion coefficient; k_b, Boltzmann's constant; η, viscosity). ^{d} Measurements for 0.01 mg mL^{-1} of MOx-NPs in water at pH 7. ^{e} Average zeta-potential values obtained from the electrophoretic mobility (U) by using the Smoluchowski equation, i.e., $\zeta = \eta U/(\varepsilon_o \varepsilon_r)$ (ε_r, dielectric constant); the errors are calculated as the standard deviation of the values from different measurements and are less than 20% of the values, unless stated explicitly.

to the field of nanoparticles. This method enables a comprehensive screening of MOx-NP interactions with optically transparent analytes, including amino acids and peptides. This is important, among others, to evaluate their biological effects as well as their potential in biocatalysis.

RESULTS

Characterization of Nanoparticles. Photophysical characterizations of the investigated metal oxide nanoparticles CuO, Co$_3$O$_4$, CeO$_2$, MgO, and TiO$_2$ were performed using UV−vis spectrophotometry and fluorescence spectroscopy. The investigated nanoparticles showed strong and continuous absorption spectra (Figure 1) but did not show any luminescence upon excitation at 280 nm, a prerequisite for the employed method involving Trp as a fluorescent label.

The data obtained from the surface characterization are shown in Table 1. The synthetic technique, flame spray pyrolysis (FSP), for synthesis of ultrafine particles is described elsewhere.[36,37] The selected MOx-NPs have average particle diameters in the range of 5−13 nm and surface areas between 87 and 164 m^2 g^{-1}. Additionally, transmission electron microscopic (TEM) images of the MOx-NPs (Figure 2) confirm that the particle size of CuO, Co$_3$O$_4$, and TiO$_2$ is in the range of 10−15 nm, whereas that of CeO$_2$ is in the range of 5−10 nm.

In aqueous solution (water at pH 7), the average particle diameters ranged from 280 to 820 nm (Table 1, determined by dynamic light scattering), revealing sizable agglomeration. The agglomeration process in small particles due to weak interactions (no sintering bridges) is at equilibrium such that the actual surface area for adsorption does not change; that is, the entire surface is believed to be still available for the adsorption due to reversibility of the weakly bound agglomerates at a specific time.[38−42] The measured zeta-potential values (surface charge) of the nanoparticles were positive for CuO, Co$_3$O$_4$, and MgO and negative for TiO$_2$ and CeO$_2$. Since zeta-potential values of MOx-NPs depend strongly on the synthesis procedure as well as on the precise experimental conditions, including pH and solvent,[43−45] a comparison with literature values[6,46−51] carries limited information content.[52] In the course of our investigation, we found that MOx-NPs, in particular CuO, can partially dissolve in buffers (see Supporting Information) but not in neat water.
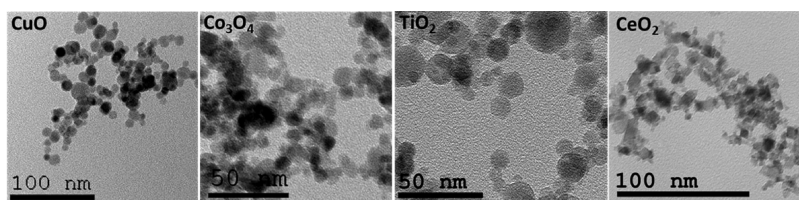
Figure 2. Transmission electron microscopic images of the investigated CuO, Co$_3$O$_4$, TiO$_2$, and CeO$_2$ nanoparticles.

Consequently, all experiments on peptide adsorption were performed in water.

Scattering Correction. The monitoring of adsorption and desorption phenomena on metal nanoparticles of the Au or Ag type by conventional optical spectroscopy is often difficult due to their strong absorption properties originating, among others, from their surface plasmon bands. Metal oxides do not absorb as strongly in the visible and/or near-UV range, in some cases not at all, which makes MOx-NPs, in principle, amenable to optical spectroscopy in water. Cuvette-based optical measurements of MOx-NPs require attention due to the strong light-scattering characteristics of the resulting dispersions. In our present study, we have applied a scattering correction as detailed in the Supporting Information. Specifically, to correct for light-scattering effects on the absorption, we selected benzoyl benzoic acid (BBA) as a competitive absorber, which has an absorption maximum ($\lambda_{max} = 266$ nm) close to the preferred excitation wavelength of Trp ($\lambda_{max} = 280$ nm) and which is nonfluorescent. It should be noted here that, although this scattering correction is straightforward to apply, previous studies on the fluorescence quenching by MOx-NPs lack comparable corrections,[27−29] which renders the associated results quantitatively less meaningful.

Effect of MOx-NPs on Tryptophan and Its Derivatives. First, the interactions of different MOx-NPs with the free amino acid Trp, its 5-fluoro derivative 5F-Trp, and its acetylated, amidated, and ester derivatives, namely, *N*-acetyl tryptophan, tryptophan amide, and tryptophan methyl ester, were monitored. Expectedly, the addition of MOx-NPs caused an apparent quenching of Trp fluorescence. However, after correction for the fluorescence loss originating from scattering of the MOx-NP solutions (eq S1 in Supporting Information), the fluorescence intensity of the tryptophan *derivatives* remained constant, within an error range of ±5%, up to relatively high OD values of 0.4 (Figure 3). This suggests that the fluorescence decrease was due to the light scattering and not due to molecular interactions (adsorption, fluorescence quenching).

In the case of Trp and 5F-Trp and only with CuO, quenching was observed even after the scattering correction (Figure 4). This can be attributed to the chelating nature of the zwitterions toward Cu(II) sites that is not present in the Trp derivatives. The absence of quenching of Trp by the other nanoparticles could
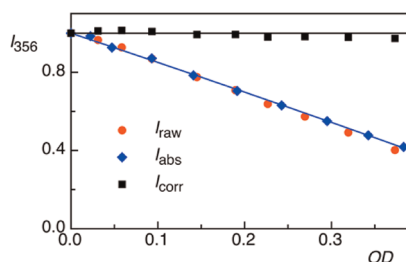

Figure 3. Decrease in fluorescence intensity of tryptophan amide at 356 nm (I_{raw}, red) upon addition of CuO. The blue line shows the loss in fluorescence intensity upon addition of benzoyl benzoic acid (BBA) as a competitive absorber (I_{abs}, blue, fitted by a linear function). The black line shows the fluorescence intensity corrected for light scattering (I_{corr}, black) according to eq S1 of the Supporting Information.[53]
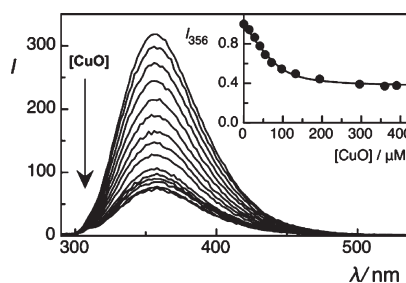

Figure 4. Changes in fluorescence spectra ($\lambda_{ex} = 280$ nm) of tryptophan (5 μM) upon addition of CuO. The inset shows the fitting (by using a 1:1 binding model; see text) for the corrected fluorescence intensity at 356 nm plotted against the apparent concentration of MOx-NPs, converted to μM.

be due to the lower affinity of these metal centers as compared to copper.[54,55] For our investigation of peptides with N-terminal Trp and amidated C-terminus, the interaction of tryptophan amide was important. The fact that tryptophan amide did not show any fluorescence loss upon addition of the MOx-NPs provided strong circumstantial evidence that the indole chromophore itself does not show any significant adsorption on the investigated MOx-NPs, but that the adsorption is driven by other amino acid side chains and/or the extended peptide backbone.

Interactions of Nanoparticles with Peptides. We selected peptides composed of a Trp residue at the N-terminal end followed by six identical amino acid residues. Such peptides are sufficiently short to ensure robust solid-phase synthesis and to maintain sufficient solubility also for relatively hydrophobic residues such as alanine, while being sufficiently long to expose the character of
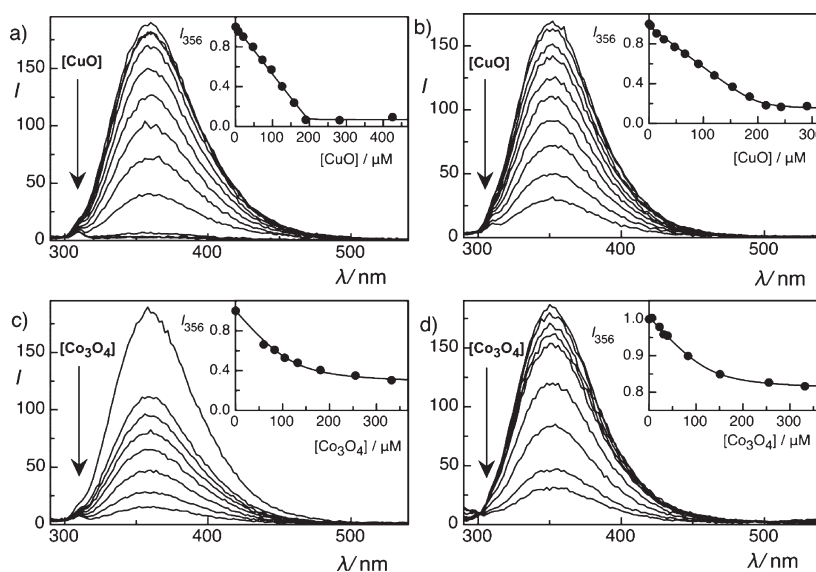
Figure 5. Changes in fluorescence spectra (λ_{ex} = 280 nm) of (a) 5F-TrpHis$_6$-NH$_2$ (5 μM) and (b) TrpAsp$_6$-NH$_2$ (5 μM) upon addition of CuO, as well as of (c) 5F-TrpHis$_6$-NH$_2$ (5 μM) and (d) TrpAsp$_6$-NH$_2$ (5 μM) upon addition of Co$_3$O$_4$; all in water at pH 7. The insets show the fitting (by using a 1:1 binding model; see text) for the corrected fluorescence intensity at 356 nm plotted against the apparent concentration of MOx-NPs, converted to μM.

the peptide backbone and differentiate them from simple amino acids.[56] The C-terminus was amidated to reduce C-terminal charge effects. The interactions of nanoparticles with alanine (TrpAla$_6$-NH$_2$), serine (TrpSer$_6$-NH$_2$), lysine (TrpLys$_6$-NH$_2$), histidine (TrpHis$_6$-NH$_2$), and aspartate (TrpAsp$_6$-NH$_2$) containing hexapeptides were investigated by monitoring the changes in their fluorescence spectra upon addition of the MOx-NPs. The fluorescence intensities of the peptides upon addition of nanoparticles, after correction for light scattering, remained constant in the presence of most MOx-NPs and for most investigated peptides. Only upon addition of CuO and Co$_3$O$_4$, the fluorescence of Trp was efficiently quenched (Figure 5). In the case of CuO, quenching was seen with all of the peptides; however, the extent of quenching depended on the type of peptide. On the other hand, in the case of Co$_3$O$_4$, significant quenching was only observed with histidine and aspartate peptides. No quenching was observed in the case of other metal oxides (see Figure S2 in the Supporting Information) and this revealed immediately a high selectivity for the interaction between the peptides and the CuO and Co$_3$O$_4$ MOx-NPs. In our earlier work, these two metal oxides have been found to be relatively toxic to living cells because of the extensive charge transfer from the cellular medium to the semiconductor, possibly due to similar surface adsorption.[57]

The quenching of the peptides, in the presence of CuO and Co$_3$O$_4$, can be assigned to adsorption of the peptides on the surface of the nanoparticles. In particular, the possibility of dynamic fluorescence quenching of the peptides by the nanoparticles can be excluded based on three independent lines of evidence.
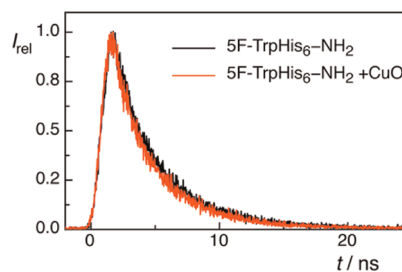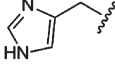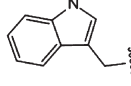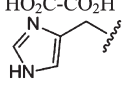

Figure 6. Fluorescence lifetime decay traces (λ_{ex} = 280 nm, λ_{em} = 350 nm) of 5F-TrpHis$_6$-NH$_2$ (5 μM) in the absence and in the presence of CuO (0.01 mg mL^{-1}) in water at pH 7 (counts were normalized).

First, the monomeric model compound, tryptophan amide, as well as several other Trp-containing peptides showed no comparable fluorescence quenching, although the possibility of dynamic quenching by the nanoparticles would be identical. Second, the fluorescence *lifetimes* of the peptides remained unchanged in the presence of the nanoparticles (Figure 6), which along with the dramatic changes in the fluorescence intensities (also gauged from a decreased photon count in the time-resolved measurements) provided compelling evidence for a static quenching, as it would occur, in particular, when the chromophore is adsorbed on the surface of the nanoparticles. Third, while the corrected fluorescence intensity was reduced, it did not vanish but reached a plateau region at higher nanoparticle concentrations, particularly for Trp/CuO case (see Figure 4). This demonstrates that a new state is formed (the peptide−nanoparticle aggregate), which displays a reduced, but nonvanishing fluorescence intensity; for dynamic quenching, increasing concentrations would always increase the amount of quenching.

TABLE 2. Apparent Binding Constants of Different Polypeptides and Low Molecular Weight Biological Analytes with CuO and Co_3O_4 Nanoparticles

Analyte[a]	Residue[b]	$K/(M^{-1})$[c]	
		CuO	Co_3O_4
5F–TrpHis$_6$–NH$_2$		$> 5 \times 10^{10}$	$(1.9 \pm 0.6) \times 10^6$
5F–TrpHis$_6$–NH$_2$ (pH 1)[d]		$< 10^2$	
TrpAsp$_6$–NH$_2$	–CH$_2$-COOH	$(1.5 \pm 1.2) \times 10^7$	2.3×10^6
TrpAla$_6$–NH$_2$	–CH$_3$	1.9×10^5	$< 10^2$
TrpSer$_6$–NH$_2$	–CH$_2$-OH	$(1.5 \pm 0.6) \times 10^7$	$< 10^2$
TrpLys$_6$–NH$_2$	–(CH$_2$)$_4$-NH$_2$	$(1.3 \pm 0.4) \times 10^6$	$< 10^2$
Trp (as amino acid)		$(3.3 \pm 0.8) \times 10^6$	$< 10^2$
Oxalate	HO$_2$C-CO$_2$H	7.2×10^{4e}	
His (as amino acid)		5.8×10^{5e}	

[a] In water at pH 7 unless stated differently. [b] Residues (R), see Scheme 1. [c] Relative apparent binding constants, calculated according to a 1:1 binding model, assuming the same number of binding sites for each analyte[33−35] and by assuming a relative concentration of the nanoparticles in M, *i.e.*, by assuming molecular weights of CuO (79.5 g mol^{-1}) and Co_3O_4 (240.8 g mol^{-1}); error ±20%, unless explicitly stated. [d] In 0.1 M hydrochloric acid, pH 1. [e] Binding constants determined by competitive fluorescence titrations.[33−35]

Because the recorded changes in corrected fluorescence intensities with respect to nanoparticle concentrations do not represent simple Stern−Volmer-type quenching plots, but rather titration plots for a chemical equilibrium (that of adsorption), they can be used to extract relative binding constants of CuO and Co_3O_4 with different peptides, respectively. Although binding stoichiometries are unknown, the data could be fitted with a standard 1:1 binding model by converting the amount of nanoparticles into an apparent "concentration" of metal oxide (Table 2) and correcting the concentration with an arbitrarily fixed factor of 0.03 to convert from concentration to apparent number of accessible binding sites. The resulting relative binding constants (Table 2, in M^{-1}) are consequently also apparent ones, which allow only a semiquantitative comparison.

On one hand, it can be stated that adsorption of TrpHis$_6$-NH$_2$ is more than 3 orders of magnitude stronger than that of TrpAsp$_6$-NH$_2$ and TrpSer$_6$-NH$_2$, but it is more than 4 orders stronger than that of TrpLys$_6$-NH$_2$ and the free amino acid Trp. TrpAla$_6$-NH$_2$ shows the weakest tendency for interaction, 5 orders of magnitude lower than that of TrpHis$_6$-NH$_2$. On the other hand, it can be seen that only 5F-TrpHis$_6$-NH$_2$ and TrpAsp$_6$-NH$_2$ adsorb on the surface of Co_3O_4 and the adsorption propensities, of the same order of magnitude for both peptides, are several orders of magnitude lower than those of CuO. From the above results, it can also been seen that Co_3O_4 is more "selective" than CuO for adsorbing specific peptides. Of course, this comparison assumes that different types of MOx-NPs have comparable surface area and size, which is at best approximately fulfilled (Table 1). The results clearly reveal the *hitherto* unknown binding preferences of different amino acid residues to the nanoparticle surface, a piece of information which is essential to understand their mechanism of interactions with proteins (which are critical for medical applications).[7,17] Efficient interactions with proteins may or may not be desirable for a particular use. In this respect, our fluorescence-based method can potentially provide a powerful tool, for example, to monitor differential binding to differently doped or otherwise functionalized MOx-NPs.

After identification of the most strongly binding peptide motif (hexahistidine), we proceeded to optimize the method. For this purpose, we exchanged Trp by 5F-Trp during solid-phase peptide synthesis. Indeed, fluorescence quenching for 5F-TrpHis$_6$-NH$_2$ upon addition of CuO and Co_3O_4 was observed, and the absolute amount exceeded that observed for TrpHis$_6$-NH$_2$, resulting in a virtually quantitative fluorescence quenching of the adsorbed peptides. This enhanced fluorescence response is greatly advantageous for more accurate monitoring of the adsorption (and desorption, see below) process. Accordingly, the 5F-TrpHis$_6$-NH$_2$ peptide was preferred in the subsequent measurements. The extracted binding constants of the two peptides were comparable, which revealed that it was the hexahistidine backbone, and not the N-terminal Trp residue, which drives the adsorption process (see below). The differential fluorescence response between Trp and 5F-Trp also provides
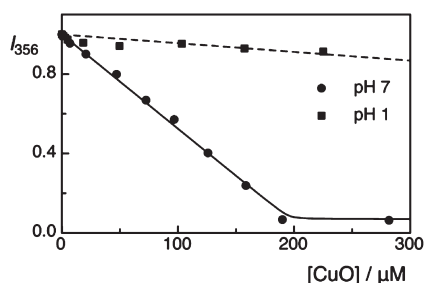
Figure 7. Effect of pH on fluorescence quenching of 5F-TrpHis$_6$-NH$_2$ (5 μM) upon addition of CuO at pH 7 (bottom) and pH 1 (top).

	ζ (mV)[a]				
additive	CuO	Co$_3$O$_4$	TiO$_2$	MgO	CeO$_2$
none	22	10	−17	14	−27
TrpAsp$_6$-NH$_2$	−32	−31	−26	−16	−31
TrpLys$_6$-NH$_2$	23	15.6	23	16	23
5F-TrpHis$_6$-NH$_2$	4.2	5	9.1	2.0	0.9 ± 0.3
TrpAla$_6$-NH$_2$	4.1 ± 1.3	16 ± 7	−17	13 ± 4	−11
TrpSer$_6$-NH$_2$	1.8	1.7	−22	7.6	−8 ± 4

[a] Error ±20% unless stated explicitly, calculated as standard deviation of the values from repeated measurements.

important mechanistic information on the quenching process. In particular, the enhanced fluorescence quenching suggests that the singlet-excited state of Trp is deactivated by an electron transfer from the nanoparticle (surface) to the chromophore; 5F-Trp is more electron-deficient than Trp[58] and, accordingly, undergoes photoinduced electron transfer more readily.

Furthermore, the effect of pH on the binding propensity of the 5F-TrpHis$_6$-NH$_2$ peptide with CuO was investigated. Interestingly, at lower pH (pH 1.0), insignificant fluorescence quenching of the peptide was observed upon addition of CuO (see Figure 7). This was not due to the coating of the nanoparticle surface by chloride ions which was established by the lack of displacement of the peptide by (sodium) chloride (up to 20 mM) in a control experiment (data not shown). It rather suggests that the affinity of the hexahistidine peptide to adsorb on the MOx-NPs is pH-dependent, as would be expected from the fact that the charge of the histidine residue (pK_a = 6.04)[59] can easily be tuned by changing the pH of the solution.

Effect of Hexapeptides on Zeta-Potential Values. To corroborate the actual adsorption of the peptides on the nanoparticle surfaces, we have also measured the zeta-potential values of different MOx-NPs in the absence and presence of the hexapeptides (Table 3), which afforded characteristic differences in zeta-potential values. In general, the zeta-potential of most of the MOx-NPs remained constant, within error, except upon addition of the charged peptides where an inversion of the surface charge was observed upon addition of the oppositely charged peptide. Changes were also seen for peptides carrying the same surface charge, although these were not as large as those observed for the oppositely charged ones. The interactions between similarly charged components have been reported previously and are expected to be favorable due to a combination of non-electrostatic interactions (hydrophobic, hydrogen bonding, van der Waals, and steric interactions).[60] The changes in the zeta-potential upon addition of serine and alanine peptides can also be explained based on the non-electrostatic argument. Furthermore, the changes upon addition of similarly charged peptides might also be due to counterion-enhanced multilayer

formation, thus exposing the peptide charge at the surface.[61]

Competitive Binding of Analytes Followed by Indicator Displacement. Any fluorophore, which produces a fluorescence response upon undergoing a *reversible* binding event, can in principle be exploited to monitor the competitive binding of other ("invisible") analytes. The addition of these analytes leads to an inversion of the original fluorescence response, which can be similarly monitored and employed to extract the binding constant, now of the analyte. This method is known as "indicator displacement assay", which is well-established in the areas of biological chemistry, where it is broadly used to measure, for example, antigen–antibody binding,[62] as well as in supramolecular chemistry, where it is frequently used to determine the complexation by synthetic receptors,[34,63,64] prominently macrocyclic host molecules.[33,65,66] In the case of the Trp-containing peptides investigated herein, their binding causes a fluorescence quenching such that the addition of analyte causes a fluorescence increase ("recovery"), as illustrated in Scheme 2. As a limitation of the method, the added analytes should not show strong absorption bands at 280 nm, where Trp is being excited.

Since carboxylates have been invoked in forming chelates with many metal ions,[48] we selected oxalate as the simplest dicarboxylate for the displacement experiments. We selected TrpAsp$_6$-NH$_2$ as the "indicator peptide", whose binding is strong but not too tight (Table 2). Indeed, upon addition of sodium oxalate to a solution of the preformed TrpAsp$_6$-NH$_2$·CuO peptide/nanoparticle aggregate, a fluorescence enhancement was observed (see Figure 8b). For the next set of experiments, histidine was chosen based on its known affinity toward transition metals.[68,69] The addition of the amino acid histidine to a solution of TrpAsp$_6$-NH$_2$·CuO led similarly to a fluorescence recovery (Figure 8a). In both cases, the fluorescence intensity approached a plateau region at high concentrations of competitor. The extracted binding constants of the "monomeric" analytes oxalate and histidine were, however, 3 and 2 orders of magnitude lower than for
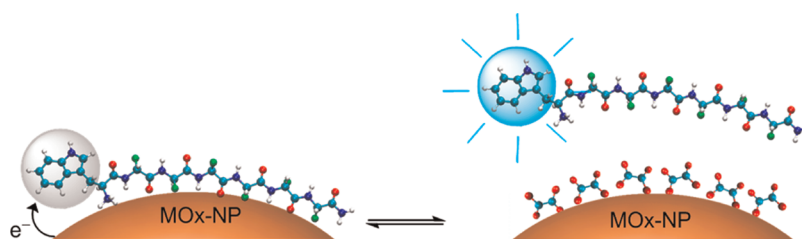
Scheme 2. Fluorescence response of Trp-containing polypeptides adsorbed on MOx-NPs upon addition of a competitive analyte (sodium oxalate in this case).
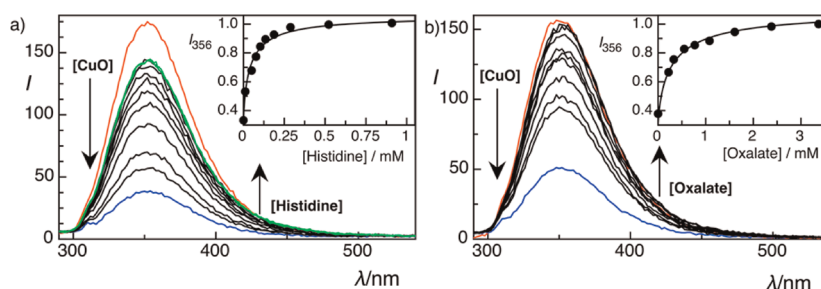

Figure 8. Change in the fluorescence spectra of TrpAsp$_6$-NH$_2$·CuO upon addition of (a) histidine and (b) sodium oxalate. The fitting (using a competitive binding model) for the fluorescence intensity at 356 nm plotted against the concentration of competitor is shown in the inset. Note that binding constants were determined by assuming relative concentrations of the nanoparticles in μM. Fluorescence intensities of the peptide (red spectra), which decreased upon addition of nanoparticles (blue spectra), were (partially) recovered upon addition of analyte up to a maximum analyte concentration of 0.91 mM for histidine and 3.37 mM for oxalate (green spectra).[67]

the hexaaspartate and hexahistidine peptides, respectively (Table 2), which shows that the presence of several side chains (negatively charged or histidine) is greatly beneficial to affect strong adsorption. This hints to a cooperative effect of several amino acid side chains in the MOx-NP adsorption. The binding in the case of amino acids is mainly driven by the chelating nature of the α-amino and carboxylate functional groups. Thus, a comprehensive screening with all different amino acids was not performed since the binding constants would be expected to be of the same order of magnitude as that of tryptophan.

DISCUSSION

Emerging nanotechnology applications in the fields of medicine and biology entail the use of nanoparticles for probing biological processes and structures as well as for constructing sophisticated nanoscale drug delivery systems.[70,71] Metal oxide nanoparticles (MOx-NPs), for example, are already in use for an entire range of applications in food industry, cosmetics (*e.g.*, sunscreens), drug delivery, and biomedicine (*e.g.*, contrast agents for MRI).[9−14,70−73] Thus, adsorption studies of peptides may not only provide fundamental information about elementary biomolecule−surface interactions but also enable identification of specific chemical groups participating in such adsorption processes. Furthermore, biomolecule nanoparticle interactions will inevitably determine their fate within cells and tissues *in vivo*, such that the precise mode of their interaction is important for understanding their biological responses, such as their toxicology.

Herein, we introduce the use of fluorescently labeled peptides to study adsorption of short polypeptides on surfaces of MOx-NPs. The selection of our model peptides was based on the nature of side chains of amino acids: hexaalanine is hydrophobic, hexaserine is uncharged polar, hexalysine is positively charged, and hexaaspartate is negatively charged. Due to the pK_a value of histidine (pK_a = 6.04), hexahistidine is expected to be highly positively charged at strongly acidic pH, but neutral near physiological pH, where it is also known to act as a nitrogenous ligand for transition metals. It should be noted here that the detection of analyte−nanoparticle interactions by fluorescence presents a highly sensitive technique; in our present experiments, only 5 μM of peptide (analyte) was generally required. Analytical techniques which require millimolar concentrations of analytes, such as FT-IR, are, in fact, unsuitable for the investigation of many biomolecules.[6,20,22]

Our results reveal that the adsorption of the peptides on the surface of MOx-NPs depends on two main factors: (1) type and charge status of the side chains of the polypeptides and (2) type of MOx-NPs. Only CuO and Co$_3$O$_4$ were "active" in adsorbing and quenching the selected peptides. The absence of fluorescence quenching by TiO$_2$, MgO, and CeO$_2$ could be due to two reasons: either there is no adsorption or there is adsorption, but no associated fluorescence response. Since the two causes cannot be differentiated, adsorption of the peptidic analytes on these types of nanoparticles cannot be investigated by means of the present
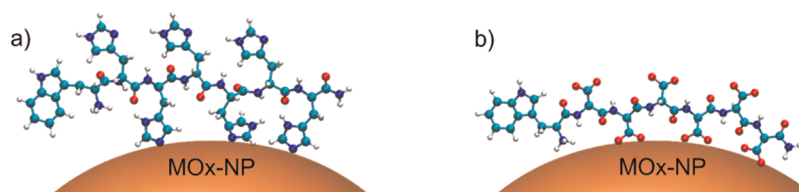
Scheme 3. Proposed molecular interactions for the adsorption of (a) histidine and (b) aspartate peptides on the surface of MOx-NPs.

technique. The photophysically active metal oxides (CuO or Co_3O_4) give rise to a semiconductor–liquid interphase in solution. The adsorption of the proteins on the surface of the NPs was therefore expected to induce charge transfer across the interphase and to cause band bending due to the formation of a space-charge layer near the valence band of the semi-conductor.[57] This could be another reason why CuO and Co_3O_4 were active in the selective adsorption and quenching of the peptides on the surface.

Protein chemosorption could be mediated by co-ordinative bond formation between the metal center and the electron donor group from the protein surface. Transition-metal ions (electron pair acceptors) considered as Lewis acids and electronegative species (electron donors) as Lewis bases present in the chelating ligand are involved in complex formation. The affinity of a protein for a metal chelate depends strongly on the metal ion involved in the coordination. For the adsorption of proteins with an iminodiacetic acid chelating group, the affinities of many proteins toward metal centers are known to be in the following order: $Cu^{2+} > Ni^{2+} > Zn^{2+} \geq Co^{2+}$.[54,55] Similarly, for the (neutral) histidine-containing peptides investigated herein, a strong interaction was observed for CuO and Co_3O_4 nanoparticles.

The possible motifs of polypeptide binding are sketched in Scheme 3. The observed strong adsorption of the 5F-TrpHis$_6$-NH$_2$ peptide on CuO and Co_3O_4 nanoparticles is likely due to the intrinsic affinity of the nitrogen atoms in the (neutral) imidazole ring to form metal–ligand bonds with transition metals. The fact that the binding of 5F-TrpHis$_6$-NH$_2$ with CuO is greatly reduced in acidic solution (Figure 7) supports the interpretation of this molecular interaction. The affinity of histidine for transition metals is, in fact, well-known for peptides, where "polyhistidine tags" with 5–6 histidines at one terminus are rationally exploited for protein purification and binding assays by using chromatographic separation techniques with transition-metal (predominantly Ni or Co)-containing stationary phases.[74,75] The affinity of polyhistidine tags is known to be micromolar,[69] perfectly in line with the binding constants obtained from our direct nanoparticle–peptide titrations (Table 2). The interactions between 5F-TrpHis$_6$-NH$_2$ and CuO as well as Co_3O_4 present therefore an example of a polyhistidine–nanoparticle interaction. The fact that the polypeptide

TrpAsp$_6$-NH$_2$ can be displaced by addition of the amino acid histidine (up to 1 mM, Figure 8a) is also reminiscent—just at the nanoparticle level—of the procedure in polyhistidine tag assays, where imidazolium (0.8–80 mM) is added to liberate the protein.[76] On the basis of our present results, MOx-NPs could also be employed for peptide and protein purification, for example, by using magnetic nanoparticle variants[77,78] to allow mechanical separation from solutions.

The observed adsorption of the TrpAsp$_6$-NH$_2$ peptide on nanoparticles, although several orders of magnitude weaker, as well as the non-negligible adsorption of oxalate, also weaker than that of histidine (Table 2), shows that interactions between carboxylate groups and MOx-NP surfaces cannot be neglected. This adsorption to the nanoparticle surfaces can be attributed either to electrostatic interactions (negatively charged analyte bound to positively charged surface) and/or to a coordinative bond formation between the carboxylate group with the transition metals at the metal surface. If only an electrostatic interaction was important, one might also expect an adsorption onto the positively surface-charged MgO (Table 1) for which our fluorescence-based technique provided, however, no indication. The obtained results for CuO and Co_3O_4 therefore point to the formation of weak coordinative bonds with carboxylate groups, similar to those observed for the imidazolium ring.

The interaction with the other peptides (seen only in the case of CuO) could be due to the higher binding affinity of copper, as stated earlier. The higher binding constants obtained for hexaaspartate and hexaserine show that the adsorption is enhanced in the case of polar peptides compared to the nonpolar peptides like hexaalanine. On the other hand, the comparable binding constants obtained for hexalysine and the free amino acid Trp point toward the involvement of the nitrogen of the side chain in the adsorption. Different MOx-NPs may, of course, have an affinity for different functional groups and charges, or they may adsorb only large proteins but not polypeptides, which will require follow-up studies. Similarly, it needs to be emphasized here that MOx-NPs (synthesized by techniques other than the presently used flame spray pyrolysis) display different surface reactivity, particle shape, size, and surface curvature.[79,80] This may also result in different adsorption propensity and selectivity toward peptides and proteins, which can now be investigated by our method, as well.

CONCLUSION

We have investigated the interaction of metal oxide nanoparticles with selected hexapeptides by fluorescence spectroscopy. The adsorption of the peptides on the nanoparticle surface depends mainly on the side chains of the amino acids in the polypeptides; more than 5 orders of magnitude variation in affinity in dependence on the amino acid was observed, with histidine being the most strongly adsorbing one. From a methodological point of view, the fluorescence quenching of the tryptophan residue offers a convenient method to quantify the adsorption of tryptophan-containing peptides and, potentially, proteins. While presently an intrinsic fluorescent probe was chosen, tryptophan could be, in principle, substituted by alternative chromophores, which could offer higher sensitivity in terms of fluorescence quantum yield (that of Trp is moderate, with 0.14 in water)[81] or better quenching efficiency, as demonstrated herein by selecting 5-fluorotryptophan. The reversibility of the adsorption further allows the construction of fluorescent indicators, which can be first bound to the nanoparticle surface and then displaced by analytes of interest. This enables one to quantify the binding of analytes, which cannot be monitored directly by optical spectroscopy, as shown herein for oxalate and histidine. Similar to the use of fluorescence-based displacement assays in pharmacological screening, the method can be miniaturized, is convenient, robust, and up-scalable to high-throughput format, which could be of interest, for example, to assess the binding of different medicinally relevant peptides or of substrates for catalytic applications. Furthermore, the selectivity and reversibility of these adsorption processes could be potentially exploited for protein purification.

MATERIALS AND METHODS

Tryptophan, N-acetyl tryptophan, tryptophan methyl ester, tryptophan amide, sodium oxalate, histidine, and 4-benzoyl benzoic acid were purchased from Fluka Chemie or Sigma Aldrich. The peptides were commercially synthesized in >95% purity (Biosyntan, Berlin). Millipore water was used for most experiments, and the pH was adjusted using HCl and NaOH accordingly. The pH was measured ($\pm$0.1 units) with a pH meter (WTW 330i) equipped with a WTW SenTix Mic glass electrode. The concentrations of the peptide solutions were determined from the absorption of the peptide solutions at 280 nm using a molar extinction coefficient of 5500 M^{-1} cm^{-1} for tryptophan and 5700 M^{-1} cm^{-1} for 5-fluorotryptophan.[82] For the titration experiments, the peptide solutions were titrated with MOx-NP solutions containing an identical concentration of peptide (to prevent concentration changes in the course of the titration). The pH of both solutions was adjusted to 7 $\pm$ 0.1 before the titration, where required, to exclude effects of pH variations. In addition, the pH of the final solution (i.e., after titration) was measured to ensure there was no pH change during the titration.

The metallorganic precursors copper napthenate (1.58 g of Cu^{2+}, 0.5 M by metal, Strem Chemical, 99.9% pure), cobalt napthenate (1.47 g of Co^{2+}, 0.5 M by metal in xylene, Strem Chemical, 99.9% pure), titanium(IV) isopropoxide (1.02 g of Ti^{4+}, 0.5 M by metal, Sigma Chemical, 99.9% pure), magnesium napthenate (0.6076 g of Mg^{2+}, Strem Chemical, 99.9% pure), and cerium(III) 2-ethylhexanoate (49% in 2-ethylhexanoic acid, 3.50 g of Ce^{2+}, 0.5 M by metal) were used for the preparation of CuO, Co_3O_4, TiO_2, MgO, and CeO_2, respectively. All metallorganic precursors were dissolved in an organic solvent (xylene, 99.95%, Strem). The solutions were then delivered to the nozzle tip by a syringe pump at a flow rate of 5 mL min^{-1} by atomizing the precursor solution with dispersant O_2 at a flow rate of 5 mL min^{-1} and maintaining a pressure drop of 1.5 bar at the nozzle tip. The spray was ignited by a supporting CH_4 and O_2 premixed flame (1.5 and 3.2 L min^{-1}) forming a self-sustaining spray flame. The particles were formed by reaction, nucleation, surface growth, coagulation, and coalescence in the spray flame environment and collected by filters after the particle stream had been diluted with cold gas.[36]

The Brunauer−Emmett−Teller (BET) method for surface area measurements was carried out at 77 K by using a Quantachrome NOVA 4000e Autosorb gas sorption system to determine the specific surface areas of the samples. The powders were placed in a test cell and allowed to degas for 2 h at 200 °C in flowing nitrogen, which removes water vapor and adsorbed gases from the samples. Data were obtained by exposing or removing a known quantity of adsorbing gas into or out of a sample cell containing the solid adsorbent maintained at the constant liquid nitrogen temperature. The average particle diameters (dry) were calculated from the specific surface area.

Nanoparticle solutions were freshly prepared in the required solution and were sonicated for 40 min to ensure efficient dispersion of the nanoparticles. UV−vis measurements were performed with a Varian Cary 4000 UV−vis spectrophotometer, and the steady-state fluorescence spectra were recorded in conventional quartz cuvettes (path length of 10 mm) with a Varian Cary Eclipse instrument. Fluorescence lifetimes were obtained by time-correlated single-photon counting (Edinburgh Instruments FLS 920) by using a LDH-P-CA280 laser diode (λ_{ex} = 280 nm, λ_{em} = 350 nm, fwhm ca. 420 ps) for excitation. Size and zeta-potential values of the nanoparticles were measured by dynamic light scattering with a Zetasizer Nano Series instrument (Malvern Instruments ZEN 3600), equipped with a 633 nm laser. For the size measurements, the detector was placed at 173° (backscatter detection), whereas for the zeta-potential measurements, the beam scattered at an angle of 17° was detected. The size and zeta-potential measurements were performed in water (refractive index = 1.330, viscosity = 0.8872) at 25 °C. For the size measurements, the material parameters for refractive index and absorption were set to 1.330 and 0.01, respectively.

Conflict of Interest: The authors declare no competing financial interest.

University Bremen) for providing the initial results for the UV spectrophotometric characterization of the nanoparticles.

REFERENCES AND NOTES

1. Nel, A.; Xia, T.; Mädler, L.; Li, N. Toxic Potential of Materials at the Nanolevel. *Science* **2006**, *311*, 622–627.
2. Nel, A. E.; Mädler, L.; Velegol, D.; Xia, T.; Hoek, E. M. V.; Somasundaran, P.; Klaessig, F.; Castranova, V.; Thompson, M. Understanding Biophysicochemical Interactions at the Nano-Bio Interface. *Nat. Mater.* **2009**, *8*, 543–557.
3. Damoiseaux, R.; George, S.; Li, M.; Pokhrel, S.; Ji, Z.; France, B.; Xia, T.; Suarez, E.; Rallo, R.; Mädler, L.; *et al.* No Time To Lose—High Throughput Screening To Assess Nanomaterial Safety. *Nanoscale* **2011**, *3*, 1345–1360.
4. George, S.; Pokhrel, S.; Xia, T.; Gilbert, B.; Ji, Z.; Schowalter, M.; Rosenauer, A.; Damoiseaux, R.; Bradley, K. A.; Mädler, L.; *et al.* Use of a Rapid Cytotoxicity Screening Approach To Engineer a Safer Zinc Oxide Nanoparticle through Iron Doping. *ACS Nano* **2009**, *4*, 15–29.
5. Zhang, H. Z.; Penn, R. L.; Hamers, R. J.; Banfield, J. F. Enhanced Adsorption of Molecules on Surfaces of Nanocrystalline Particles. *J. Phys. Chem. B* **1999**, *103*, 4656–4662.
6. Mudunkotuwa, I. A.; Grassian, V. H. Citric Acid Adsorption on TiO_2 Nanoparticles in Aqueous Suspensions at Acidic and Circumneutral pH: Surface Coverage, Surface Speciation, and Its Impact on Nanoparticle–Nanoparticle Interactions. *J. Am. Chem. Soc.* **2010**, *132*, 14986–14994.
7. Vallee, A.; Humblot, V.; Pradier, C.-M. Peptide Interactions with Metal and Oxide Surfaces. *Acc. Chem. Res.* **2010**, *43*, 1297–1306.
8. Pettibone, J. M.; Cwiertny, D. M.; Scherer, M.; Grassian, V. H. Adsorption of Organic Acids on TiO_2 Nanoparticles: Effects of pH, Nanoparticle Size, and Nanoparticle Aggregation. *Langmuir* **2008**, *24*, 6659–6667.
9. Battez, A. H.; González, R.; Viesca, J. L.; Fernández, J. E.; Fernández, J. M. D.; Machado, A.; Chou, R.; Riba, J. CuO, ZrO_2 and ZnO Nanoparticles as Antiwear Additive in Oil Lubricants. *Wear* **2008**, *265*, 422–428.
10. Jammi, S.; Sakthivel, S.; Rout, L.; Mukherjee, T.; Mandal, S.; Mitra, R.; Saha, P.; Punniyamurthy, T. CuO Nanoparticles Catalyzed C–N, C–O, and C–S Cross-Coupling Reactions: Scope and Mechanism. *J. Org. Chem.* **2009**, *74*, 1971–1976.
11. Reddy, V. P.; Kumar, A. V.; Swapna, K.; Rao, K. R. Copper Oxide Nanoparticle-Catalyzed Coupling of Diaryl Diselenide with Aryl Halides under Ligand-Free Conditions. *Org. Lett.* **2009**, *11*, 951–953.
12. Rout, L.; Jammi, S.; Punniyamurthy, T. Novel CuO Nanoparticle Catalyzed C–N Cross Coupling of Amines with Iodobenzene. *Org. Lett.* **2007**, *9*, 3397–3399.
13. Rout, L.; Sen, T. K.; Punniyamurthy, T. Efficient CuO-Nanoparticle-Catalyzed C–S Cross-Coupling of Thiols with Iodobenzene. *Angew. Chem., Int. Ed.* **2007**, *46*, 5583–5586.
14. Stoimenov, P. K.; Klinger, R. L.; Marchin, G. L.; Klabunde, K. J. Metal Oxide Nanoparticles as Bactericidal Agents. *Langmuir* **2002**, *18*, 6679–6686.
15. Lundqvist, M.; Stigler, J.; Cedervall, T.; Berggård, T.; Flanagan, M. B.; Lynch, I.; Elia, G.; Dawson, K. The Evolution of the Protein Corona around Nanoparticles: A Test Study. *ACS Nano* **2011**, *5*, 7503–7509.
16. Chen, H.; Su, X.; Neoh, K.-G.; Choe, W.-S. Probing the Interaction between Peptides and Metal Oxides Using Point Mutants of a TiO_2-Binding Peptide. *Langmuir* **2008**, *24*, 6852–6857.
17. Deng, Z. J.; Mortimer, G.; Schiller, T.; Musumeci, A.; Martin, D.; Minchin, R. F. Differential Plasma Protein Binding to Metal Oxide Nanoparticles. *Nanotechnology* **2009**, *20*, 455101.
18. Gertler, G.; Fleminger, G.; Rapaport, H. Characterizing the Adsorption of Peptides to TiO_2 in Aqueous Solutions by Liquid Chromatography. *Langmuir* **2010**, *26*, 6457–6463.
19. Monti, S.; Carravetta, V.; Battocchio, C.; Iucci, G.; Polzonetti, G. Peptide/TiO_2 Surface Interaction: A Theoretical and Experimental Study on the Structure of Adsorbed ALA-GLU and ALA-LYS. *Langmuir* **2008**, *24*, 3205–3214.
20. Roddick-Lanzilotta, A. D.; McQuillan, A. J. An *In Situ* Infrared Spectroscopic Investigation of Lysine Peptide and Polylysine Adsorption to TiO_2 from Aqueous Solutions. *J. Colloid Interface Sci.* **1999**, *217*, 194–202.
21. Methivier, C.; Lebec, V.; Landoulsi, J.; Pradier, C.-M. Probing the Binding Mechanism of Peptides on a Copper Surface: Multilayer Self-Assembly Promoted by Glutamate Residues. *J. Phys. Chem. C* **2011**, *115*, 4041–4046.
22. Peng, Z. G.; Hidajat, K.; Uddin, M. S. Adsorption of Bovine Serum Albumin on Nanosized Magnetic Particles. *J. Colloid Interface Sci.* **2004**, *271*, 277–283.
23. Monti, S.; Alderighi, M.; Duce, C.; Solaro, R.; Tiné, M. R. Adsorption of Ionic Peptides on Inorganic Supports. *J. Phys. Chem. C* **2009**, *113*, 2433–2442.
24. Dringen, R.; Koehler, Y.; Derr, L.; Tomba, G.; Schmidt, M. M.; Treccani, L.; Ciacchi, L. M.; Rezwan, K. Adsorption and Reduction of Glutathione Disulfide on α-Al_2O_3 Nanoparticles: Experiments and Modeling. *Langmuir* **2011**, *27*, 9449–9457.
25. Wigginton, N. S.; de Titta, A.; Piccapietra, F.; Dobias, J.; Nesatyy, V. J.; Suter, M. J. F.; Bernier-Latmani, R. Binding of Silver Nanoparticles to Bacterial Proteins Depends on Surface Modifications and Inhibits Enzymatic Activity. *Environ. Sci. Technol.* **2010**, *44*, 2163–2168.
26. Hu, J.; Song, Z.; Chen, L.; Yang, H.; Li, J.; Richards, R. Adsorption Properties of MgO(111) Nanoplates for the Dye Pollutants from Wastewater. *J. Chem. Eng. Data* **2010**, *55*, 3742–3748.
27. Wang, Y.-Q.; Zhang, H.-M.; Zhou, Q.-H.; Xu, H.-L. A Study of the Binding of Colloidal Fe_3O_4 with Bovine Hemoglobin Using Optical Spectroscopy. *Colloids Surf., A* **2009**, *337*, 102–108.
28. Kathiravan, A.; Anandan, S.; Renganathan, R. Interaction of Colloidal TiO_2 with Human Serum Albumin: A Fluorescence Quenching Study. *Colloids Surf., A* **2009**, *333*, 91–95.
29. Kathiravan, A.; Renganathan, R. Interaction of Colloidal TiO_2 with Bovine Serum Albumin: A Fluorescence Quenching Study. *Colloids Surf., A* **2008**, *324*, 176–180.
30. Fairbairn, E. A.; Keller, A. A.; Mädler, L.; Zhou, D.; Pokhrel, S.; Cherr, G. N. Metal Oxide Nanomaterials in Seawater: Linking Physicochemical Characteristics with Biological Response in Sea Urchin Development. *J. Hazard. Mater.* **2011**, *192*, 1565–1571.
31. Busch, W.; Bastian, S.; Trahorsch, U.; Iwe, M.; Kühnel, D.; Meissner, T.; Springer, A.; Gelinsky, M.; Richter, V.; Ikonomidou, C.; *et al.* Internalisation of Engineered Nanoparticles into Mammalian Cells *in Vitro*: Influence of Cell Type and Particle Properties. *J. Nanopart. Res.* **2011**, *13*, 293–310.
32. Lakowicz, J. R. *Principles of Fluorescence Spectroscopy*; Springer: New York, 2006.
33. Bailey, D. M.; Hennig, A.; Uzunova, V. D.; Nau, W. M. Supramolecular Tandem Enzyme Assays for Multiparameter Sensor Arrays and Enantiomeric Excess Determination of Amino Acids. *Chem.—Eur. J.* **2008**, *14*, 6069–6077.
34. Bakirci, H.; Nau, W. M. Fluorescence Regeneration as a Signaling Principle for Choline and Carnitine Binding: A Refined Supramolecular Sensor System Based on a Fluorescent Azoalkane. *Adv. Funct. Mater.* **2006**, *16*, 237–242.
35. Hennig, A.; Bakirci, H.; Nau, W. M. Label-Free Continuous Enzyme Assays with Macrocycle-Fluorescent Dye Complexes. *Nat. Methods* **2007**, *4*, 629–632.
36. Pokhrel, S.; Birkenstock, J.; Schowalter, M.; Rosenauer, A.; Mädler, L. Growth of Ultrafine Single Crystalline WO_3 Nanoparticles Using Flame Spray Pyrolysis. *Cryst. Growth Des.* **2010**, *10*, 632–639.
37. Teoh, W. Y.; Amal, R.; Mädler, L. Flame Spray Pyrolysis: An Enabling Technology for Nanoparticles Design and Fabrication. *Nanoscale* **2010**, *2*, 1324–1347.
38. Allen, E.; Smith, P.; Henshaw, J. A Review of Particles Agglomeration. U.S. Department of Energy, **2001**; pp 1–42.

39. Frandsen, C.; Mørup, S. Reversible Aggregation and Magnetic Coupling of α-Fe₂O₃ Nanoparticles. *J. Phys.: Condens. Matter* **2006**, *18*, 7079.

40. Yang, L.; Guo, C.; Jia, L.; Xie, K.; Shou, Q.; Liu, H. Fabrication of Biocompatible Temperature- and pH-Responsive Magnetic Nanoparticles and Their Reversible Agglomeration in Aqueous Milieu. *Ind. Eng. Chem. Res.* **2010**, *49*, 8518–8525.

41. Klabunde, K. J.; Richards, R. *Nanoscale Materials in Chemistry*; John Wiley & Sons, Inc.: New York, 2009.

42. Richards, R.; Li, W.; Decker, S.; Davidson, C.; Koper, O.; Zaikovski, V.; Volodin, A.; Rieker, T.; Klabunde, K. J. Consolidation of Metal Oxide Nanocrystals. Reactive Pellets with Controllable Pore Structure That Represent a New Family of Porous, Inorganic Materials. *J. Am. Chem. Soc.* **2000**, *122*, 4921–4925.

43. Mandzy, N.; Grulke, E.; Druffel, T. Breakage of TiO₂ Agglomerates in Electrostatically Stabilized Aqueous Dispersions. *Powder Technol.* **2005**, *160*, 121–126.

44. Mao, J. A.; Bai, Y.; Gu, L.; van Aken, P. A.; Tu, M. J. Preparation and Characterization of Size-Controlled CeO₂ Nanoparticles Coated with SiO₂. *J. Nanopart. Res.* **2010**, *12*, 2045–2049.

45. Wang, W.-Y.; Ku, Y. Effect of Solution pH on the Adsorption and Photocatalytic Reaction Behaviors of Dyes Using TiO₂ and Nafion-Coated TiO₂. *Colloids Surf., A* **2007**, *302*, 261–268.

46. Chang, H.; Jwo, C. S.; Lo, C. H.; Tsung, T. T.; Kao, M. J.; Lin, H. M. Rheology of CuO Nanoparticle Suspension Prepared by ASNSS. *Rev. Adv. Mater. Sci.* **2005**, *10*, 128–132.

47. Guedes, M.; Ferreira, J. M. F.; Ferro, A. C. A Study on the Aqueous Dispersion Mechanism of CuO Powders Using Tiron. *J. Colloid Interface Sci.* **2009**, *330*, 119–124.

48. Li, C.-C.; Chang, M.-H. Colloidal Stability of CuO Nanoparticles in Alkanes *via* Oleate Modifications. *Mater. Lett.* **2004**, *58*, 3903–3907.

49. Horst, A. M.; Neal, A. C.; Mielke, R. E.; Sislian, P. R.; Suh, W. H.; Mädler, L.; Stucky, G. D.; Holden, P. A. Dispersion of TiO₂ Nanoparticle Agglomerates by *Pseudomonas aeruginosa*. *Appl. Environ. Microbiol.* **2010**, *76*, 7292–7298.

50. Meng, Y. D.; Chen, D. R.; Jiao, X. L. Fabrication and Characterization of Mesoporous Co₃O₄ Core/Mesoporous Silica Shell Nanocomposites. *J. Phys. Chem. B* **2006**, *110*, 15212–15217.

51. Park, J. S.; Han, Y. H. Preparation of MgO-Coated BaTiO₃ Particles through a Surface-Induced Precipitation Method. *Ceram. Int.* **2006**, *32*, 673–677.

52. While the literature values for CuO (15 to 20 mV, from refs 46–48), CeO₂ (−20 mV, from ref 44), and TiO₂ (−17.9 to −30 mV, from refs 6 and 49) show acceptable agreement with our nanoparticle zeta-potentials, those for Co₃O₄ (−3.1 mV, in an ethanol−water−ammonia mixture from ref 50) and MgO (−2 mV, from ref 51) are smaller, with opposite signs.

53. The scattering correction based on the addition of a competitive absorber neglects scattering effects on the fluorescence emission as well as multiple backscattering effects on both absorption and emission. The former would further reduce the measured fluorescence while the latter would tend to enhance it. The fact that the scattering effect on the absorption was sufficient to correct the experimental data (Figure 3) shows that the secondary scattering effects presumably counterbalance each other. Additional care was taken by working at sufficiently low OD values (<0.4) to reduce artifacts related to reabsorption and inhomogeneous absorption.

54. Porath, J.; Olin, B. Immobilized Metal Affinity Adsorption and Immobilized Metal Affinity Chromatography of Biomaterials. Serum Protein Affinities for Gel-Immobilized Iron and Nickel Ions. *Biochemistry* **1983**, *22*, 1621–1630.

55. Prasanna, R. R.; Vijayalakshmi, M. A. Immobilized Metal-Ion Affinity Systems for Recovery and Structure-Function Studies of Proteins at Molecular, Supramolecular, and Cellular Levels. *Pure Appl. Chem.* **2010**, *82*, 39–55.

56. Huang, F.; Nau, W. M. A Conformational Flexibility Scale for Amino Acids in Peptides. *Angew. Chem., Int. Ed.* **2003**, *42*, 2269–2272.

57. Zhang, H.; Ji, Z.; Xia, T.; Meng, H.; Low-Kam, C.; Liu, R.; Pokhrel, S.; Lin, S.; Wang, X.; Liao, Y.-P.; *et al.* Use of Metal Oxide Nanoparticle Band Gap To Develop a Predictive Paradigm for Acute Pulmonary Inflammation Based on Oxidative Stress. *ACS Nano* **2012**, 10.1021/nn3010087.

58. Liu, T. Q.; Callis, P. R.; Hesp, B. H.; de Groot, M.; Buma, W. J.; Broos, J. Ionization Potentials of Fluoroindoles and the Origin of Nonexponential Tryptophan Fluorescence Decay in Proteins. *J. Am. Chem. Soc.* **2005**, *127*, 4104–4113.

59. Berg, J. M. *Biochemistry*; W.H. Freeman: New York, 2002; pp 974−975.

60. Gole, A.; Phadtare, S.; Sastry, M.; Langevin, D. Studies on Interaction between Similarly Charged Polyelectrolyte: Fatty Acid System. *Langmuir* **2003**, *19*, 9321–9327.

61. Laugel, N.; Betscha, C.; Winterhalter, M.; Voegel, J.-C.; Schaaf, P.; Ball, V. Relationship between the Growth Regime of Polyelectrolyte Multilayers and the Polyanion/Polycation Complexation Enthalpy. *J. Phys. Chem. B* **2006**, *110*, 19443–19449.

62. Kusterbeck, A. W.; Wemhoff, G. A.; Charles, P. T.; Yeager, D. A.; Bredehorst, R.; Vogel, C.-W.; Ligler, F. S. A Continuous-Flow Immunoassay for Rapid and Sensitive Detection of Small Molecules. *J. Immunol. Methods* **1990**, *135*, 191–197.

63. Anslyn, E. V. Supramolecular Analytical Chemistry. *J. Org. Chem.* **2007**, *72*, 687–699.

64. Wiskur, S. L.; Ait-Haddou, H.; Lavigne, J. J.; Anslyn, E. V. Teaching Old Indicators New Tricks. *Acc. Chem. Res.* **2001**, *34*, 963–972.

65. Bakirci, H.; Koner, A. L.; Nau, W. M. Binding of Inorganic Cations by *p*-Sulfonatocalix[4]arene Monitored through Competitive Fluorophore Displacement in Aqueous Solution. *Chem. Commun.* **2005**, 5411–5413.

66. Florea, M.; Nau, W. M. Implementation of Anion-Receptor Macrocycles in Supramolecular Tandem Assays for Enzymes Involving Nucleotides as Substrates, Products, and Cofactors. *Org. Biomol. Chem.* **2010**, *8*, 1033–1039.

67. The added analyte does not change the pH of the solution or the fluorescence of Trp, thus, the partial fluorescence recovery could be due to the formation of multiple or mixed layers of analyte and fluorescent peptide.

68. Schmitt, J.; Hess, H.; Stunnenberg, H. G. Affinity Purification of Histidine-Tagged Proteins. *Mol. Biol. Rep.* **1993**, *18*, 223–230.

69. Zoroddu, M. A.; Medici, S.; Peana, M. Copper and Nickel Binding in Multi-Histidinic Peptide Fragments. *J. Inorg. Biochem.* **2009**, *103*, 1214–1220.

70. Chertok, B.; Moffat, B. A.; David, A. E.; Yu, F. Q.; Bergemann, C.; Ross, B. D.; Yang, V. C. Iron Oxide Nanoparticles as a Drug Delivery Vehicle for MRI Monitored Magnetic Targeting of Brain Tumors. *Biomaterials* **2008**, *29*, 487–496.

71. Jain, T. K.; Morales, M. A.; Sahoo, S. K.; Leslie-Pelecky, D. L.; Labhasetwar, V. Iron Oxide Nanoparticles for Sustained Delivery of Anticancer Agents. *Mol. Pharmaceutics* **2005**, *2*, 194–205.

72. Ren, G.; Hu, D.; Cheng, E. W. C.; Vargas-Reus, M. A.; Reip, P.; Allaker, R. P. Characterisation of Copper Oxide Nanoparticles for Antimicrobial Applications. *Int. J. Antimicrob. Agents* **2009**, *33*, 587–590.

73. Nohynek, G. J.; Dufour, E. K.; Roberts, M. S. Nanotechnology, Cosmetics and the Skin: Is There a Health Risk? *Skin Pharmacol. Physiol.* **2008**, *21*, 136–149.

74. Hemdan, E. S.; Zhao, Y.-J.; Sulkowski, E.; Porath, J. Surface Topography of Histidine Residues: A Facile Probe by Immobilized Metal Ion Affinity Chromatography. *Proc. Natl. Acad. Sci. U.S.A.* **1989**, *86*, 1811–1815.

75. Rossetto, O.; Schiavo, G.; de Laureto, P. P.; Fabbiani, S.; Montecucco, C. Surface Topography of Histidine Residues of Tetanus Toxin Probed by Immobilized-Metal-Ion Affinity Chromatography. *Biochem. J.* **1992**, *285*, 9–12.

76. Janknecht, R.; Demartynoff, G.; Lou, J.; Hipskind, R. A.; Nordheim, A.; Stunnenberg, H. G. Rapid and Efficient Purification of Native Histidine-Tagged Protein Expressed by Recombinant Vaccinia Virus. *Proc. Natl. Acad. Sci. U.S.A.* **1991**, *88*, 8972–8976.

77. Grass, R. N.; Athanassiou, E. K.; Stark, W. J. Covalently Functionalized Cobalt Nanoparticles as a Platform for

Magnetic Separations in Organic Synthesis. *Angew. Chem., Int. Ed.* **2007**, *46*, 4909–4912.

78. Lu, A.-H.; Salabas, E. L.; Schüth, F. Magnetic Nanoparticles: Synthesis, Protection, Functionalization, and Application. *Angew. Chem., Int. Ed.* **2007**, *46*, 1222–1244.

79. Natile, M. M.; Ugel, E.; Maccato, C.; Glisenti, A. LaCoO$_3$: Effect of Synthesis Conditions on Properties and Reactivity. *Appl. Catal., B* **2007**, *72*, 351–362.

80. Richards, R.; Bönnemann, H. Synthetic Approaches to Metallic Nanomaterials. In *Nanofabrication Towards Biomedical Applications*; Kumar, C. S. S. R., Hormes, J., Leuschner, C., Eds.; Wiley-VCH Verlag GmbH & Co. KGaA: Weinheim, Germany, 2005; pp 3−32.

81. Lotte, K.; Plessow, R.; Brockhinke, A. Static and Time-Resolved Fluorescence Investigations of Tryptophan Analogues - A Solvent Study. *Photochem. Photobiol. Sci.* **2004**, *3*, 348–359.

82. Schuler, B.; Kremer, W.; Kalbitzer, H. R.; Jaenicke, R. Role of Entropy in Protein Thermostability: Folding Kinetics of a Hyperthermophilic Cold Shock Protein at High Temperatures Using ^{19}F NMR. *Biochemistry* **2002**, *41*, 11670–11680.